THE JOURNAL OF PHYSICAL CHEMISTRY C

Article

pubs.acs.org/JPCC

XPD and XANES Studies of $Ce_{0.9}Zr_{0.1}O_2$ Nanocatalysts under Redox and Catalytic CH_4 Oxidation Conditions

María G. Zimicz,[†] Fernando D. Prado,[†] Analía L. Soldati,[‡] Diego G. Lamas,[§] and Susana A. Larrondo*[,∥,⊥]

[†]Instituto de Física del Sur (IFISUR)-CONICET, Av. Alem No. 1253, 8000 Bahía Blanca, Buenos Aires Argentina

[‡]CONICET, Grupo Caracterización de Materiales, CAB-CNEA, Bustillo 9500, 8400 Bariloche, Argentina

[§]CONICET, Escuela de Ciencia y Tecnología, UNSAM, Campus Miguelete, 25 de Mayo y Francia, 1650 San Martín, Provincia de Buenos Aires Argentina

[∥]CINSO (Centro de Investigaciones en Sólidos), CITEDEF-UNIDEF-CONICET, J.B. de La Salle No. 4397, 1603 Villa Martelli, Pcia. de Buenos Aires Argentina

[⊥]Instituto de Investigación e Ingeniería Ambiental (3iA), UNSAM, Campus Miguelete, 25 de Mayo y Francia, 1650 San Martín, Provincia de Buenos Aires Argentina

ABSTRACT: The aim of this work is to take further insight into the structural stability of cerium−zirconium catalysts under reducing, oxidizing and reaction conditions. *In situ* synchrotron based techniques (XANES and XPD) were used in order to determine the stability of crystal structure and the oxidation state of cerium cations in the reaction conditions prevailing in the catalytic studies. *In situ* XPD studies in 5 mol % H_2 atmosphere revealed that no structural changes occur until 870 °C. At this temperature, the sample synthesized with glycine, which presents lower crystallite agglomeration, segregated a small quantity of a reduced phase. On the contrary, the solid synthesized with lysine, with more agglomerated crystallites, does not show structural changes in all the temperature range. Reoxidation treatments in 5 mol % O_2 revealed that at 750 °C the segregated phase disappears and that the original cubic structure is restored. *In situ* XANES studies in the Ce L_{III} absorption edge indicate that under catalytic reaction conditions, the degree of reduction of Ce^{4+} is low, allowing the occurrence of methane oxidation. The solid is capable to deliver the oxygen of its structure when no oxygen is fed into the reactor until the 50% of cerium cations become reduced, triggering the deactivation process. Therefore, it is clear for these studies that the Ce^{4+} to Ce^{3+} ratio in the lattice is governing the catalytic behavior of the solid. The catalytic results collected during *in situ* XANES experiments are in excellent agreement with our previous catalytic studies performed with a laboratory fixed bed reactor.

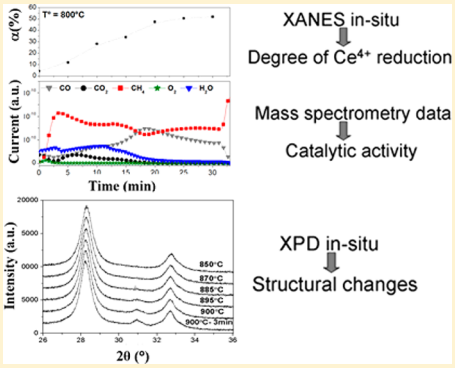

1. INTRODUCTION

ZrO_2−CeO_2 mixed oxides have been widely proposed as catalysts, supports, and anode materials for intermediate-temperature solid oxide fuel cells (IT-SOFC). The elucidation of structural and chemical changes under operating conditions has become an issue of great interest. Ceria-based catalysts attracted great attention due to ceria high reducibility and oxygen storage capacity.[1−3] In a reducing environment, cerium dioxide (CeO_2) releases oxygen to become reduced ceria (CeO_{2-x}), while in oxidizing conditions this reduced ceria can reincorporate oxygen into the crystal structure recomposing back to the cerium dioxide stoichiometry. This feature is usually called the oxygen storage capacity (OSC) and relays over the reversible redox process associated with the Ce^{4+}/Ce^{3+} redox couple. However, in ceria-based materials this reduction process from Ce^{4+} to Ce^{3+} could lead to phase segregation, depending on the doping cation, the particle size, the specific surface, the temperature, and the surrounding atmosphere. In the case of CeO_2−ZrO_2 mixed oxides, the structural studies found in the literature are limited mostly to the region corresponding to intermediate composition ($Ce_{0.5}Zr_{0.5}O_2$). Otsuka-Yao-Matsuo et al.[4] and Montini et al.[5] reported that after reducing samples of $Ce_{0.5}Zr_{0.5}O_2$ with tetragonal structure (t′), a solid with the pyrochlore structure ($Ce_2Zr_2O_7$) was obtained. Vidal et al.[6] analyzed the influence of redox treatments on $Ce_xZr_{1-x}O_2$ with low and high specific surface areas. They found that in Zr- and Ce-rich samples no modifications were detected, but for intermediate compositions appreciable phase segregation occurred. This phase segregation was apparently favored by the presintering of the mixed oxides. Rodriguez et al.[7] analyzed the physical and chemical properties of $Ce_xZr_{1-x}O_2$ (x = 0.9, 0.66, and 0.5) oxides and reported that no phase segregation occurred when the samples were heated in 5 mol % H_2 in He balance from room temperature up to 1000 °C. Similar behavior was observed by Boaro et al.[8] who found that a sample of $Ce_{0.8}Zr_{0.2}O_2$ preserves the tetragonal

Received: June 2, 2015
Revised: July 20, 2015
Published: July 28, 2015

DOI: 10.1021/acs.jpcc.5b05253
J. Phys. Chem. C 2015, 119, 19210−19217

structure after one redox cycle, evidencing only a distortion of the t″ phase structure, probably related to the promotion of reducibility of this composition.

The reduction of particle size to the nanometric level has put in evidence its influence in the structural, electronic, and chemical properties of the solids. Colon and co-workers[9] also studied the stability of CeO_2−ZrO_2 mixed oxides during oxidation processes. They suggested that the driving force for phase segregation during these treatments is the existence of a critical particle size above which the mixed oxide tends to decompose. Crystal growth would take place until a certain critical mean crystal size is reached, when phase segregation would begin forming thermodynamically more stable phases. The authors found that for $Ce_{0.5}Zr_{0.5}O_2$ samples, the critical size is around 15 nm, but it changes with sample composition. They suggested that for Ce-rich samples, the critical size would be higher.

In the Ce-rich region of the CeO_2−ZrO_2 system, it was reported that $Ce_{0.9}Zr_{0.1}O_2$ mixed oxide did not evidence any structural change in a static air atmosphere, for particle sizes in the 10−100 nm range.[10]

Therefore, the results reported are still ambiguous, and the study of structural evolution with *in situ* experiments is very valuable.

In this work, we present the analysis of structural and redox changes of $Ce_{0.9}Zr_{0.1}O_2$ mixed oxide when exposed to reducing or oxidizing flows. *In situ* X-ray diffraction and absorption techniques were performed with synchrotron light.

2. EXPERIMENTAL SECTION

2.1. Synthesis of Nanopowders. $Ce_{0.9}Zr_{0.1}O_2$ mixed oxide was synthesized by the stoichiometric α-amino acid/nitrate combustion route, starting from $ZrO(NO_3)_2{\cdot}6H_2O$ and $Ce(NO_3)_3{\cdot}6H_2O$. Glycine and lysine were used as fuels, and the obtained samples are referred to as GS and LS, respectively. After the synthesis process, the mixed oxides were calcined at 600 °C in air in order to eliminate any vestige of carbonaceous residues. The details of the synthesis process and the influence of the synthesis conditions on the textural and morphological properties of the samples was previously reported.[11]

2.2. Characterization. The texture of fresh catalysts was analyzed by N_2 physisorption in a Quantachrome Autosorb-1 equipment, obtaining the specific surface area and total pore volume of the solids. The size and morphology of the nanoparticles were analyzed using a Philips CM 200 UT microscope equipped with an ultratwin objective lens. The electron source used was a LaB6 filament operated at 200 keV. The nominal resolution was 0.2 nm for high resolution mode. The microscope was equipped with a CCD camera for digital acquisition; contrast and illumination were adjusted linearly afterward using commercially available image treatment programs. Statistics on the particles was done with the programs ITEM and Origin 8.5. Particle size is given as the mathematical average standard deviation of the largest particle dimension. In all cases more around 200 measurements were averaged, sampling in different regions of the foil.

The crystal structure of the samples under different atmospheres (5 mol % H_2/He balance, 5 mol % O_2/He balance, and 2 mol % CH_4/4 mol % O_2/He balance) was determined by *in situ* X-ray powder diffraction (XPD) technique using synchrotron radiation. The time-resolved diffraction data were collected at the D10B-XPD beamline of the Brazilian Synchrotron Light Laboratory (LNLS, Campinas, Brazil) using a high-intensity and low-resolution configuration, without crystal analyzer. The energy was set at 7997.43 eV and the X-ray wavelength was 1.55031 Å. The peak profile was not significantly affected by low resolution since the peaks are intrinsically broad. The sample powders were placed on the sample-holder inside an oven with controlled temperature. Rietveld refinements were performed with FullProfsuite open access software.[12]

In situ XANES studies were performed for the Ce L_{III}-edge in which Ce 2p electrons are excited with photons of energies above 5720 eV. These tests were carried out in the D06A-DXAS beamline of the Brazilian Synchrotron Light Laboratory. Sample preparation and method of analysis of XANES spectra were previously reported.[13] From the fitting of the absorption profile, the evolution of the degree of reduction "α" of Ce^{4+} cations when the samples were subjected to different atmospheres was obtained. The degree of reduction is defined as the Ce^{3+} to (Ce^{3+} + Ce^{4+}) atomic ratio.

During the *in situ* XPD and *in situ* XANES analyses, the inlet line of the reactor was connected to a gas-mixing station provided with mass flow controllers, and the outlet line was connected to a Pfeiffer QMS 422 Quadrupole Mass Spectrometer.

The catalytic activity experiments in total oxidation of methane of fresh solids were performed in a fixed bed reactor, laboratory scale, operated at atmospheric pressure. The experiments were performed in the 400−800 °C temperature range, with steps of 100 °C. The feed to the reactor was a mixture of 2 mol % CH_4/4 mol % O_2 and N_2 balance with a total volume flow of 333 STP $cm^3{\cdot}min^{-1}$. These studies were previously reported and are presented here for comparison purposes.[14]

3. RESULTS AND DISCUSSION

Results from N_2 physisorption experiments are listed in Table 1. It is possible to see that the α-amino acid used in the synthesis process influences the textural characteristics of the nanopowders. Sample GS exhibits higher specific surface area and pore volume and lower degree of agglomeration (D_{BET}/D_{XRD}) than sample LS.

Table 1. N_2 Physisorption Results

sample name	specific surface area, A (m^2/g)	degree of agglomeration D_{BET}/D_{XRD}[a]	total pore volume, V (cm^3/g)
GS	45 (2)	2.2 (1)	0.086 (4)
LS	4.9 (3)	22 (1)	0.011 (6)

[a]$D_{BET} = 6/A\rho$; ρ = theoretical density; D_{XRD} = crystallite size obtained by Scherrer equation.

3.1. TEM. Figure 1 shows the TEM images obtained for samples GS and LS, and the corresponding histograms for particle size distribution.

Sample GS shows a broader particle size distribution around the mean grain size of 14.7 ± 4.8 nm. This value is much higher than the determined by XPD technique. In the case of sample LS, the grain size distribution is narrower around a mean size of 7.6 ± 3.1 nm, being this value compatible with that obtained from XPD experiments. Besides, sample LS looks very agglomerated.

3.2. *In Situ* XPD Experiments. Fresh samples exhibited cubic crystal structure corresponding to the *Fm*3*m* space group.

DOI: 10.1021/acs.jpcc.5b05253
J. Phys. Chem. C 2015, 119, 19210−19217

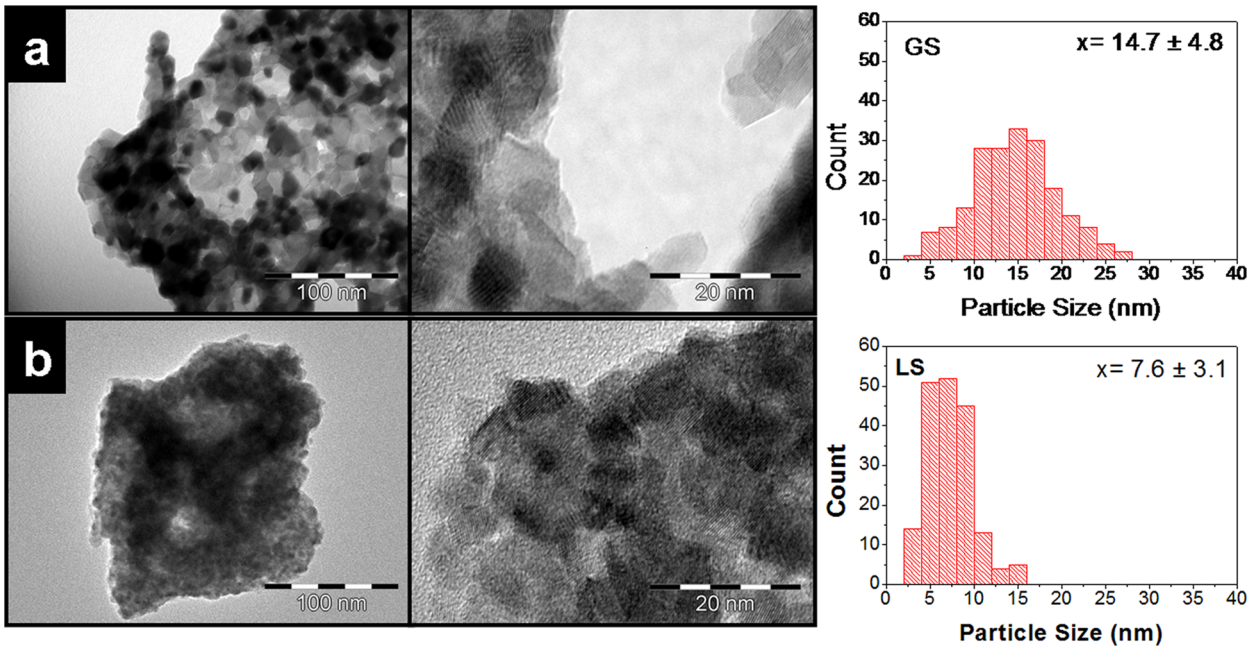

Figure 1. TEM images with two magnifications and particle size distribution for fresh samples (a) GS and (b) LS.

The average crystallite size was calculated from the width of the (111) Bragg peak using the Scherrer equation, $D = 0.9\lambda[\beta \cos(\theta)]^{-1}$, where D is the crystallite size, λ is the radiation wavelength, β is the peak width at half-maximum intensity, and θ is the Bragg angle. No influence of the α-amino acid used in the synthesis on the crystallite size (D_{XRD}) was observed.

The solids were heated with a heating ramp of 10 °C·min^{-1} under a reducing flow (5 mol % H_2/He balance, 50 STP cm^3·min^{-1}) from room temperature up to 900 °C with isothermal steps at 25, 300, 450, 600, 750, and 900 °C. The diffraction patterns were collected in the $2\theta = 20 - 80°$ angular range during the isothermal steps. In Figure 2 the cell parameters and the crystallite size evolution during the reduction process are summarized. Cell parameters for fresh samples are in agreement with values reported in the literature.[15−17] As it was said in previous sections, mean grain size for fresh LS sample is consistent with results obtained from TEM. However, for sample GS, particle size from TEM is higher than that obtained by XPD. This discrepancy can be attributed to microstrain, which produces a greater broadening in the diffraction peak and then causing a relatively smaller estimation of the crystallite size than the observed in TEM micrographs.

As temperature is increased, increments in cell parameter and crystallite size are observed, in agreement with results reported for CeO_2.[18] The increment in the cell parameter is related to the expansion of the unit cell induced by the partial reduction of Ce^{4+} to Ce^{3+}, which according to Shannon and Prewitt[19] have cationic radii, for the 8-fold coordination, of 0.97 Å (Ce^{4+}) and 1.14 Å (Ce^{3+}), respectively. The initial average crystallite sizes are in the 5−6 nm range. Around 750 °C the size starts to increase reaching a value in the 6−7 nm range at 900 °C, with an increment of nearly 25% for sample GS and above 50% for sample LS. This different behavior is a consequence of the different agglomeration ratio of the two powders. Sample LS has a much higher agglomeration ratio that favors the development of sintering necks and crystallite growth. As it was previously reported, the agglomeration ratio is strongly influenced by the α-amino acid used in synthesis, which governs the speed of the gel autoignition.[11] It is important to address that the size growth of the crystallites is much lower than observed by other authors, who reported increments reaching 300% at 900 °C for the same composition but different synthesis methods, pointing out the higher thermal stability of samples synthesized by gel-combustion method.[20]

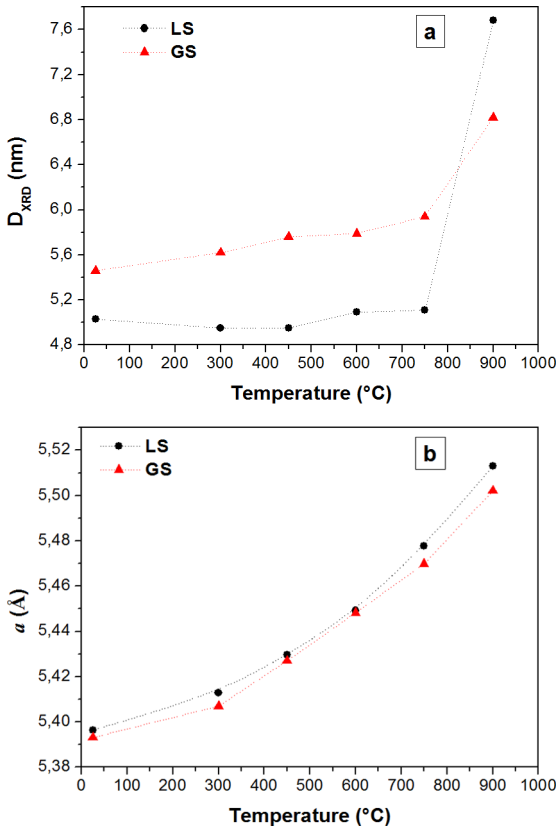

Figure 2. Variation of structural parameters with temperature in reducing atmosphere: (a) variation of D_{XRD} and (b) variation of cell parameter "a".

DOI: 10.1021/acs.jpcc.5b05253
J. Phys. Chem. C 2015, 119, 19210−19217

From the diffraction patterns collected on heating in reducing atmosphere, it is clear that sample LS retains the cubic structure in all the temperature range (Figure 3).

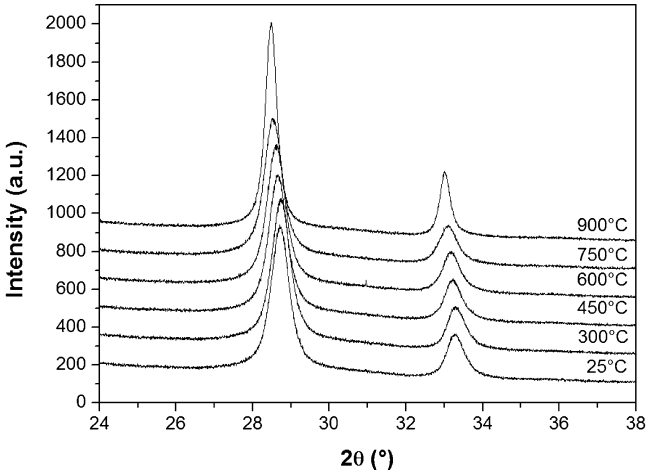

Figure 3. Diffraction patterns of sample LS collected during reduction process.

However, sample GS evidences phase segregation at 900 °C. At this temperature, a new "reduced" phase coexists with the original cubic structure. Perrichon et al.[21] reported that when CeO_2 is reduced at temperatures above 800 °C, an expanded CeO_{2-x} phase and cubic and hexagonal Ce_2O_3 phases are formed. Bernal et al.,[22] who observed segregation of Ce_2O_3 from CeO_2 during reduction at 1000 °C, addressed similar results. In our case, due to the low intensity and resolution of the peaks assigned to the "reduced" phase, it was not possible to determine its structure and composition with certainty, but they likely correspond to a reduced CeO_{2-x} phase. Even when well-crystallized phases are present, it is difficult to establish the structure with certainty. Boaro et al.[23] investigated the structural properties of $Ce_{0.5}Zr_{0.5}O_2$ mixed oxide, before and after redox treatments. By XRD and Raman analysis they found that the original symmetry of the t″ phase is lost upon reduction at 1273 K and a new phase is being formed. They were unable to fully define the new structure; however, they suggested that there is a coexistence of tetragonal and pseudopyrochlore phases. The pyrochlore structure in ceria−zirconia mixed oxides is usually reported to form at high temperature under reducing conditions.

In order to determine the temperature of segregation of the new phase during reduction treatment, shorter diffraction patterns were collected for sample GS in the 2θ = 26−36° region, where the main peak of the segregated phase appeared. The data collection was fast enough to ensure a temperature change below 10 °C during each pattern collection. The obtained results are plotted in Figure 4. It is clear that the reduced phase appears in the 885−895 °C range.

To determine whether the process was reversible or not, a reoxidation treatment was performed afterward. The sample GS was cooled down to room temperature in the former reducing atmosphere, and then was heated up to 900 °C with the same temperature program used in the reduction process, in an oxidizing flow of 5 mol %O_2/He balance (50 STP $cm^3 \cdot min^{-1}$). The diffraction patterns were collected at the intermediate isothermal steps. In Figure 5 it is possible to observe that the reduced phase persists at temperatures below 750 °C, while at

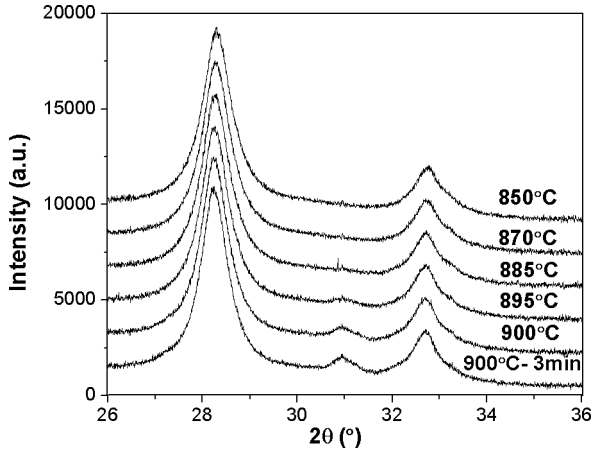

Figure 4. Diffraction patterns of sample GS collected during reduction process.

this temperature the reduced phase disappeared and the original cubic phase was recovered. In a previous *in situ* XANES study of reduction and reoxidation processes of sample GS, we found that the complete reoxidation of Ce^{3+} cations is reached at 750 °C.[13] This result is pointing out that the segregated phase disappears when cerium cations are totally reoxidized, confirming that the segregated phase is a reduced ceria phase. In our previous paper we have also reported that even though samples GS and LS have the same composition and crystal structure, the reduction and reoxidation processes of these samples are very different, suggesting the influence of crystallite size and agglomeration grade on them. At 800 °C, sample GS reached a 34% of reduction, while the sample LS suffered a reduction of 39%. From XPD studies it is clear that no phase segregation takes place in both samples until 800 °C. However, structural stability of sample LS seems to be greater since there is no segregation of secondary phases up to 900 °C. The different behavior observed between the two samples may be due to the higher degree of agglomeration of the crystallites in the sample LS, allowing a faster rate of crystallite growth (Figure 1) and an easier accommodation within the structure of the Ce^{3+} cations generated in the reduction process.

Finally, *in situ* XPD and XANES studies were also performed in operating conditions (gas flow, feed composition, temperature, etc.) similar to those used in previous catalytic experiments performed in our laboratory with a fixed-bed reactor. In this case, the samples were heated at 10 °C/min from room temperature up to 750 °C, with isothermal steps at 25, 450, 600, and 750 °C, in a mixture of 2 mol % CH_4 and 4 mol % O_2 (He balance). Diffraction patterns were collected during the isothermal periods. No structural changes were detected in sample LS. Sample GS also retained the cubic structure, but an additional peak centered at 26.5° appeared from temperature 450 °C (Figure 6). This peak was assigned to graphitic carbon formed during methane oxidation, according the ICSD number 52230.

Carbon formation can occur both by decomposition of methane (eq 1) and by the Boudouard reaction (eq 2). It is important to remark that eq 1 is highly endothermic and then favored at high temperature. On the contrary, Boudard reaction is exothermic and carbon formation is favored at temperatures below 550 °C.

$$CH_4 \leftrightarrow C + 2H_2 \quad (1)$$

DOI: 10.1021/acs.jpcc.5b05253
J. Phys. Chem. C 2015, 119, 19210−19217

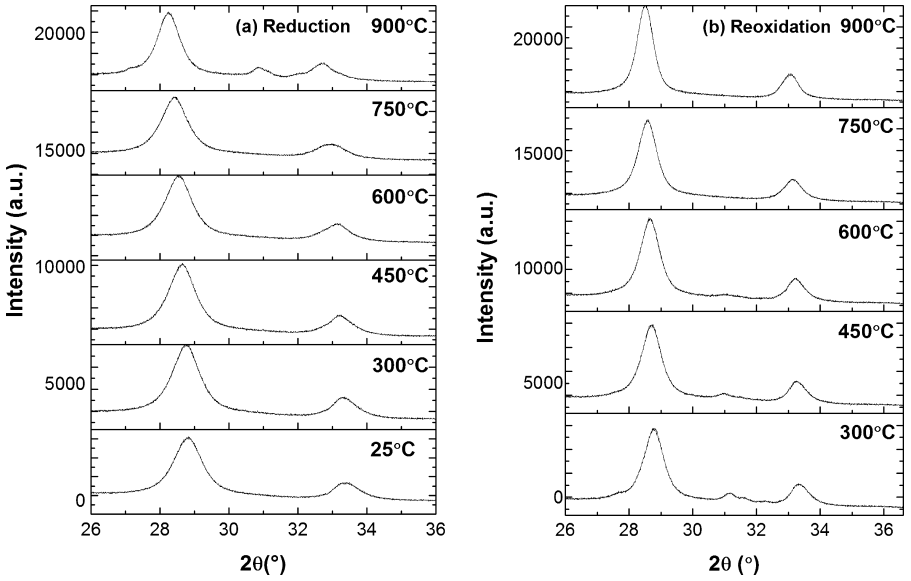

Figure 5. Diffraction patterns of sample GS collected during (a) reduction and (b) reoxidation processes.

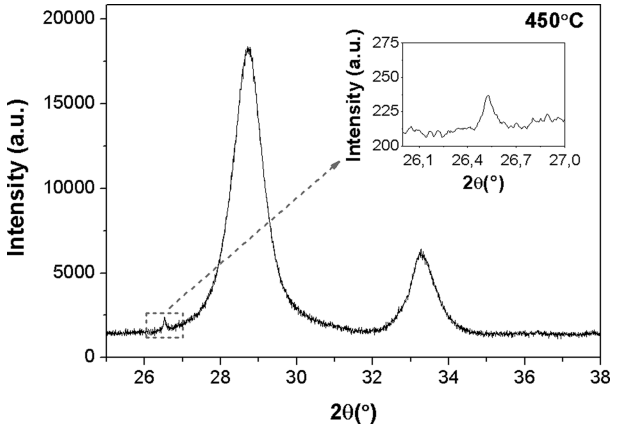

Figure 6. XPD pattern for sample GS collected during methane oxidation at 450 °C.

$$2CO \leftrightarrow C + CO_2 \quad (2)$$

From mass spectrometry data collected during the *in situ* XPD studies (Figure 7), it can be observed that oxidation products are detected from 400 °C, approximately. The signal corresponding to carbon monoxide starts to appear at 450 °C, and its signal increases with temperature increment. Therefore, the carbon deposits could be possibly produced through eq 2.

3.3. *In Situ* XANES Experiments. *In situ* XANES experiments were performed at the Ce L_{III}-edge (see Figure 8). A temperature ramp of 10 °C/min and a feed consistent of 2 mol % CH_4 and 4 mol % O_2 diluted in He were used. XANES spectra were collected from room temperature up to 800 °C. After 30 min at 800 °C, oxygen was removed from the feed to the reactor, and for 30 min XANES spectra were collected in this atmosphere of 10 mol % CH_4/He. XANES spectra were fitted as a linear combination of standard spectra, as it was previously reported.[13,18] XANES experiments in methane oxidation conditions were conducted only for sample GS, due to the poor catalytic activity of sample LS previously observed in conventional catalytic tests.[14] In Figure 9a it is shown the degree of reduction versus time on stream corresponding to these experiments, and in Figure 9b, mass spectrometry data collected during the whole experiment are plotted.

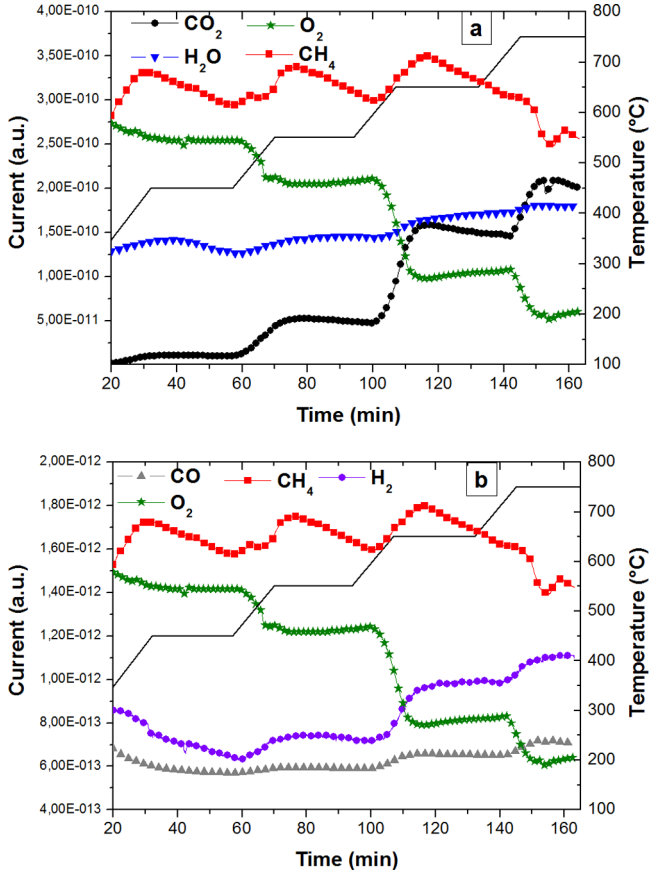

Figure 7. Mass spectrometry data collected during *in situ* XPD studies in methane oxidation conditions, for sample GS. (a) Mass spectrometry data for CO_2, H_2O, CH_4, and O_2. (b) Mass spectrometry data for CO, H_2, CH_4, and O_2.

During reaction in the feed containing CH_4 and O_2 the solid showed a very low degree of reduction reaching a steady state with a percentage of reduction, "α", of 5%. In this situation, a dynamic equilibrium between reduction and reoxidation of

DOI: 10.1021/acs.jpcc.5b05253
J. Phys. Chem. C 2015, 119, 19210−19217

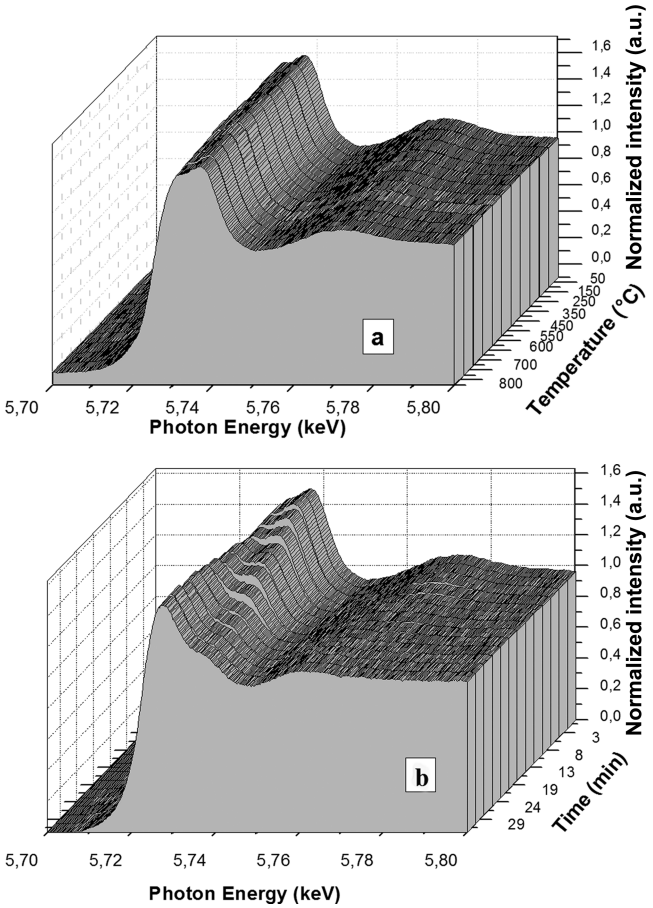

Figure 8. In situ XANES spectra at the Ce L_{III} edge, for sample GS in atmosphere of 2% CH_4–4% O_2. (a) Spectra collected from room temperature up to 800 °C; (b) spectra isothermally collected at 800 °C.

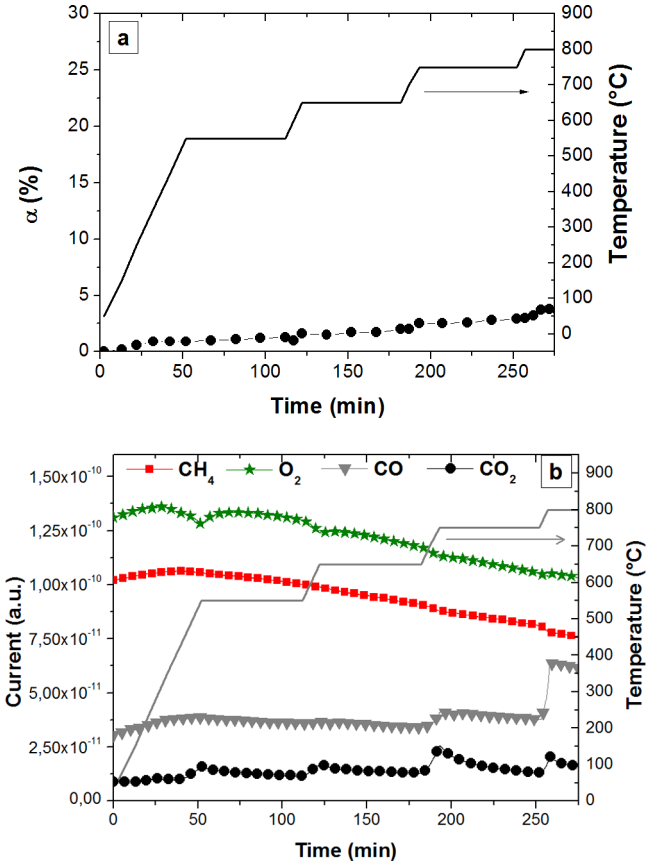

Figure 9. (a) Degree of reduction of ceria cations, evaluated from XANES spectra, vs time on stream during methane total oxidation experiments (feed composition CH_4/O_2 = 1:2). (b) Mass spectrometry data collected during the experiments.

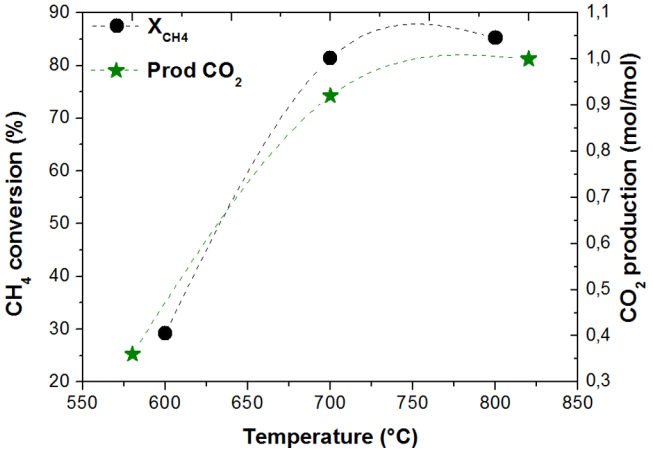

Figure 10. CH_4 conversion and CO_2 production for sample GS, with feed composition corresponding to methane total oxidation reaction.

Ce^{4+} cations was achieved, which allows the occurrence of methane total oxidation. Spectrometry data (Figure 9b) showed the continuous decrease of CH_4 and O_2 signals, evidencing the catalytic activity of the solid for methane oxidation. Total oxidation products (CO_2 and H_2O) are prevalent in the low temperature range. At approximately 650 °C a small quantity of CO is detected, indicating that methane partial oxidation is a secondary reaction.

Our previous catalytic results (Figure 10) obtained in our laboratory with a fixed bed reactor have shown an excellent performance, reaching 80% of methane conversion at 700 °C in a feed composition consisting of 2 mol % CH_4 and 4 mol % O_2 (N_2 balance), being the methane total oxidation the prevalent reaction in all the temperature range.

The only carbonated product detected in the effluent gas was carbon dioxide (CO_2). Probably carbon monoxide (CO) was not detected due to the lower sensitivity of the gas-chromatography technique compared with mass spectrometry. Besides, carbon balance between feed and effluent was in the 100% ± 5% range with no observation of traces of carbon deposits in the scanning electron microscopy micrographs of the spent catalysts.[14]

As it was mentioned above, mass spectrometry data collected during *in situ* XPD studies reveals that methane total oxidation starts at 400 °C, and methane partial oxidation at 450 °C, approximately. These temperatures are lower than those observed during *in situ* XANES analyses due to differences in sample preparation. In XPD studies, the samples are in powder form, with a good contact between gas-phase and active sites leading to a greater contact time. In XANES analyses the samples are prepared by mixing the powders with boron nitride and pressed into self-supporting discs, so the sample is diluted leading to a lower contact time, and active sites are less accessible than in XPD experiments.

After stabilizing the temperature at 800 °C, the oxygen was removed from the feed, and XANES spectra were collected

DOI: 10.1021/acs.jpcc.5b05253
J. Phys. Chem. C 2015, 119, 19210–19217

during the following 30 min. In Figure 11 it can be seen that when there is no oxygen in the feed, the catalyst begins to

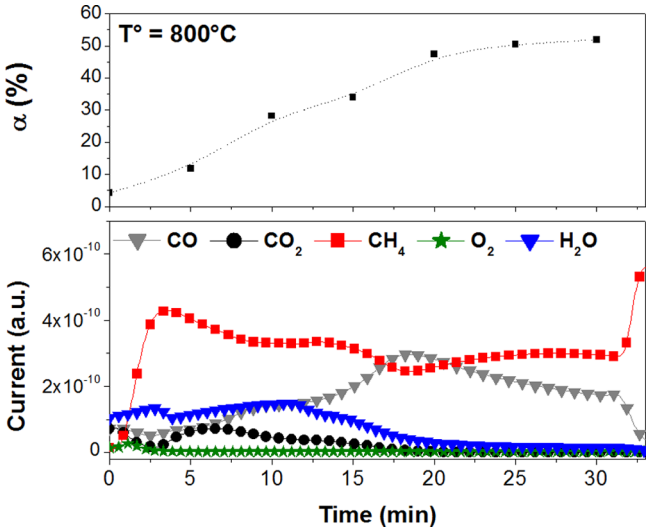

Figure 11. (a) Degree of reduction of ceria cations, evaluated from XANES spectra vs time on stream and (b) mass spectrometry data, for sample GS after removing O_2, in 10 mol % CH_4/He at 800 °C.

deliver oxygen from its structure, suffering a consequent reduction. This behavior is maintained until the solid reaches a maximum level of reduction and it deactivates. From mass spectrometry data, it can be observed that in the first minutes without oxygen, the oxygen delivered from the solid is enough to produce the total oxidation of methane. As sample reduction continues, the capability of delivering oxygen reduces, and the signal of total oxidation products (CO_2 and H_2O) starts to decrease, while carbon monoxide signal becomes predominant. When the solid reaches a maximum reduction percentage (~50%), an abrupt decrease of all the reaction products and an increase in the CH_4 signal is detected, indicating the deactivation of the catalyst. The degree of reduction reached at the end of the experiment is consistent with the previously reported maximum reduction reached in 5 mol % H_2–He balance atmosphere observed by XANES experiments.[13]

These results confirm the capability of the ceria–circonia catalyst to activate the methane molecule and exchange the lattice oxygen with methane leading to water and carbon oxides. The other important conclusion is that this capability remains until 50% of Ce^{4+} reduction is reached, which means that 25% of the oxygen atoms are released. It is worth to mention that the reduction of two Ce^{4+} cations to Ce^{3+} releases one oxygen atom. Depending on the oxygen content in the mixed oxide, we can observe the prevalence of products corresponding to total or partial oxidation of methane. This is an indication that Ce^{4+} to Ce^{3+} ratio governs the activity of the material.

4. CONCLUSIONS

From *in situ* XPD experiments, we observed a higher growth of average crystallite size in sample synthesized with lysine as α-amino acid (LS) than in that synthesized with glycine (GS) due to the higher degree of agglomeration, which facilitates the sintering process. As it was previously reported, the agglomeration ratio is strongly influenced by the α-amino acid used in the synthesis process.

From the diffraction patterns collected on heating in reducing atmosphere, it is clear that sample LS retains the cubic structure in all the temperature range, while sample GS evidences the segregation of a reduced ceria-based phase at temperature in the 885–895 °C range. We confirmed that this segregation is reversed by reoxidation. We believe that the agglomeration of the crystallites plays an important role in phase segregation. The more agglomerated solid (LS) shows a faster rate of crystallite growth that facilitates the accommodation of Ce^{3+} cations within the structure.

In situ XANES studies confirmed our previous catalytic results obtained by conventional catalytic tests in a fixed-bed reactor indicating that sample GS is an excellent catalyst for total oxidation of methane. *In situ* XANES studies in Ce-L_{III} absorption edge pointed out that the cerium cations were reduced up to a 5 mol % during the oxidation of methane, reaching a stable condition. Furthermore, it was possible to confirm that the solid is capable to deliver the oxygen of its structure when no oxygen is fed into the reactor. In this last case, the catalyst maintains its catalytic activity for a limited period of time, while cerium cations are reduced. This process continues until 50% of cerium cations become reduced, triggering the deactivation process. Therefore, it is clear for these studies that the Ce^{4+} to Ce^{3+} ratio in the lattice is governing the catalytic behavior of the solid, which operates according to the Mars–Van Krevelen model, exchanging the oxygen of the lattice with the methane molecule.

AUTHOR INFORMATION

Corresponding Author

*Tel: +54.11.4709-8158. E-mail: slarrondo@citedef.gob.ar or slarrondo@unsam.edu.ar.

Notes

The authors declare no competing financial interest.

ACKNOWLEDGMENTS

This work was supported by the Brazilian Synchrotron Light Laboratory (LNLS) under proposals D06A-DXAS-9949 and XRD1-14413, Agencia Nacional de Promoción Científica y Tecnológica (Argentina, PICT 2010 No. 0322, PICT 2013 No. 1493, PICT 2013 No. 1587, PICT 2013 No. 1032) and Ministerio de Defensa (PIDDEF No. 011/11). A.S. acknowledges the valuable support of Dr. H. Troiani (CONICET, Metals Division, Bariloche Atomic Centre) in the TEM measurements.

REFERENCES

(1) Terribile, D.; Trovarelli, A.; de Leitenburg, C.; Primavera, A.; Dolcetti, G. Catalytic Combustion of Hydrocarbons with Mn and Cu-Doped Ceria–Zirconia Solid Solutions. *Catal. Today* **1999**, *47*, 133–140.

(2) Bozo, C.; Guilhaume, N.; Garbowski, E.; Primet, M. Combustion of Methane on CeO_2–ZrO_2 Based Catalysts. *Catal. Today* **2000**, *59*, 33–45.

(3) Pengpanich, S.; Meeyoo, V.; Rirksomboon, T. Catalytic Oxidation of Methane Over CeO_2-ZrO_2 Mixed Oxide Solid Solution Catalysts Prepared Via Urea Hydrolysis. *Appl. Catal., A* **2002**, *234*, 221–233.

(4) Otsuka-Yao-Matsuo, S.; Omata, T.; Izu, N.; Kishimoto, H. Oxygen Release Behavior of $CeZrO_4$ Powders and Appearance of New Compounds κ and t*. *J. Solid State Chem.* **1998**, *138*, 47–54.

(5) Montini, T.; Bañares, M. A.; Hickey, N.; Di Monte, R.; Fornasiero, P.; Kaspar, J.; Graziani, M. Promotion of Reduction in

DOI: 10.1021/acs.jpcc.5b05253
J. Phys. Chem. C 2015, 119, 19210–19217

Ce0.5Zr0.5O2: The Pyrochlore Structure as Effect Rather Than Cause. *Phys. Chem. Chem. Phys.* **2004**, *6*, 1−3.
(6) Boaro, M.; Desinan, S.; Abate, C.; Ferluga, M.; de Leitenburg, C.; Trovarelli, A. Study on Redox, Structural and Electrical Properties of $Ce_XZr_{1-X}O_2$ for Applications in SOFC Anodes. *J. Electrochem. Soc.* **2011**, *158* (2), P22−P29.
(7) Vidal, H.; Kašpar, J.; Pijolat, M.; Colon, G.; Bernal, S.; Cordón, A.; Perrichon, V.; Fally, F. Redox Behavior of CeO_2−ZrO_2 Mixed Oxides: II. Influence of Redox Treatments on Low Surface Area Catalysts. *Appl. Catal., B* **2001**, *30*, 75−85.
(8) Rodriguez, J. A.; Wang, X.; Liu, G.; Hanson, J. C.; Hrbek, J.; Peden, C. H. F.; Iglesias-Juez, A.; Fernández-García, M. Physical and Chemical Properties of $CE_{1-X}ZR_XO_2$ Nanoparticles and $Ce_{1-X}Zr_XO_2$ (1 1 1) Surfaces: Synchrotron-Based Studies. *J. Mol. Catal. A: Chem.* **2005**, *228*, 11−19.
(9) Colon, G.; Valdivieso, F.; Pijolat, M.; Baker, R. T.; Calvino, J. J.; Bernal, S. Textural and Phase Stability of $Ce_XZr_{1-X}O_2$ Mixed Oxides Under High Temperature Oxidising Conditions. *Catal. Today* **1999**, *50*, 271−284.
(10) Zhang, F.; Hanson, J. C.; Robinson, R. D.; Herman, I. P.; Siu-Wai, C. Phases in Ceria−Zirconia Binary Oxide $(1-X)CeO_2$−$XZrO_2$ Nanoparticles: The Effect of Particle Size. *J. Am. Ceram. Soc.* **2006**, *89* (3), 1028−1036.
(11) Zimicz, M. G.; Fábregas, I. O.; Lamas, D. G.; Larrondo, S. A. Effect of Synthesis Conditions on The Nanopowder Properties of $Ce_{0.9}Zr_{0.1}O_2$. *Mater. Res. Bull.* **2011**, *46* (6), 850−857.
(12) Rodríguez-Carvajal, J. Fullprof Suite, version 2007.
(13) Zimicz, M. G.; Larrondo, S. A.; Prado, R. J.; Lamas, D. G. Time-resolved in Situ XANES Study of The Redox Properties of $Ce_{0.9}Zr_{0.1}O_2$ Mixed Oxides. *Int. J. Hydrogen Energy* **2012**, *37* (19), 14881−14886.
(14) Zimicz, M. G.; Lamas, D. G.; Larrondo, S. A. $Ce_{0.9}Zr_{0.1}O_2$ Nanocatalyst: Influence of Synthesis Conditions in The Reducibility and Catalytic Activity. *Catal. Commun.* **2011**, *15*, 68−73.
(15) Acuña, L. M.; Fuentes, R. O.; Fantini, M. C. A.; Lamas, D. G. Relation Between Distortions in The Oxygen Sublattice and The Local Order of Zr in Nanostructured ZrO_2−CeO_2 Mixed Oxides. *J. Phys. Chem. C* **2014**, *118*, 11445−11453.
(16) Kaneko, H.; Taku, S.; Tamaura, Y. Reduction Reactivity of CeO_2-ZrO_2 Oxide Under High O_2 Partial Pressure in Two-Step Water Splitting Process. *Sol. Energy* **2011**, *85*, 2321−2330.
(17) Fornasiero, P.; Di Monte, R.; Rao, G. R.; Kaspar, J.; Meriani, S.; Trovarelli, A.; Graziani, M. Rh-Loaded CeO_2-ZrO_2 Solid-Solutions as Highly Efficient Oxygen Exchangers: Dependence of The Reduction Behavior and The Oxygen Storage Capacity on The Structural-Properties. *J. Catal.* **1995**, *151*, 168−177.
(18) Alayoglu, S.; An, K.; Melaet, G.; Chen, S.; Bernardi, F.; Wang, L. W.; Lindeman, A. E.; Musselwhite, N.; Guo, J.; Liu, Z.; Marcus, M. A.; Somorjai, G. A. Pt-Mediated Reversible Reduction and Expansion of CeO_2 in Pt Nanoparticle/Mesoporous CeO_2 Catalyst: In Situ X-Ray Spectroscopy and Diffraction Studies Under Redox (H_2 and O_2) Atmospheres. *J. Phys. Chem. C* **2013**, *117*, 26608−26616.
(19) Shannon, R. D.; Prewitt, C. T. Effective Ionic Radii in Oxides and Fluorides. *Acta Crystallogr., Sect. B: Struct. Crystallogr. Cryst. Chem.* **1969**, *25*, 925−1048.
(20) Rodriguez, J. A.; Hanson, J. C.; Kim, J. Y.; Liu, G.; Iglesias-Juez, A.; Fernández-García, M. Properties of CeO_2 and $Ce_{1-X}Zr_XO_2$ Nanoparticles: X-Ray Absorption Near-Edge Spectroscopy, Density Functional, and Time-Resolved X-Ray Diffraction Studies. *J. Phys. Chem. B* **2003**, *107* (15), 3535−3543.
(21) Perrichon, V.; Laachir, A.; Bergeret, G.; Frety, R.; Toumayan, L.; Touret, O. Reduction of Cerias with Different Textures by Hydrogen and Their Reoxidation by Oxygen. *J. Chem. Soc., Faraday Trans.* **1994**, *90*, 773−781.
(22) Bernal, S.; Blanco, G.; Cauqui, M. A.; Cifredo, G. A.; Pintado, J. M.; Rodriguez-Izquierdo, J. M. Influence of Reduction Treatment on The Structural and Redox Behaviour of Ceria, La/Ce and Y/Ce Mixed Oxides. *Catal. Lett.* **1998**, *53* (1−2), 51−57.
(23) Boaro, M.; Pappacena, A.; Abate, C.; Ferluga, M.; Llorca, J.; Trovarelli, A. Effect of Redox Treatments on $Ce_{0.5}Zr_{0.5}O_2$ Based Solid Oxide Fuel Cell Anodes. *J. Power Sources* **2014**, *270*, 79−91.

DOI: 10.1021/acs.jpcc.5b05253
J. Phys. Chem. C 2015, 119, 19210−19217